

A self-organizing robotic aggregate using solid and liquid-like collective states

Baudouin Saintyves,^{1*} Matthew Spenko,² Heinrich M. Jaeger^{1,3}

¹James Franck Institute, University of Chicago, Chicago, IL 60637, USA

²Mechanical, Materials, and Aerospace Engineering,
Illinois Institute of Technology, Chicago, IL 60614, USA

³Department of Physics, University of Chicago, Chicago, IL 60637, USA

*To whom correspondence should be addressed; E-mail: saintyves@uchicago.edu.

Designing robotic systems that can change their physical form factor as well as their compliance to adapt to environmental constraints remains a major conceptual and technical challenge. To address this, we introduce the Granulobot, a modular system that blurs the distinction between soft, modular, and swarm robotics. The system consists of gear-like units that each contain a single actuator such that units can self-assemble into larger, granular aggregates using magnetic coupling. These aggregates can reconfigure dynamically and also split up into subsystems that might later recombine. Aggregates can self-organize into collective states with solid- and liquid-like properties, thus displaying widely differing compliances. These states can be perturbed locally via actuators or externally via mechanical feedback from the environment to produce adaptive shape shifting in a decentralized manner. This in turn can generate locomotion strategies adapted to different conditions. Aggregates can

move over obstacles without using external sensors or coordinate to maintain a steady gait over different surfaces without electronic communication among units. The modular design highlights a physical, morphological form of control that advances the development of resilient robotic systems with the ability to morph and adapt to different functions and conditions.

Introduction

The development of autonomous and efficient agents that can adapt to a variety of environments and perform different functions by reconfiguring their body is one of the frontiers in the field of robotics. There is an increasing need for systems that offer multi-functional, self-assembling, highly compliant capabilities in concert with resilience and robustness (1). To this end, while traditional robotic design tends to distinguish and separate components dealing with sensing, actuation, computation, and communication, a alternative strategy distributes components that each integrate these functions (2). For instance, modular design approaches replace a single mechanical body with an aggregate of multi-functional subunits that can assemble and couple together (3–6). However, this coupling often leads to rigid connections between docked units, which then implies that changes of the overall aggregate shape require an iterative reconfiguration process whereby units need to disconnect, move, and then reconnect at another location. This is incompatible with a variable mechanical compliance of the overall structure and limits adaptability to changing tasks or environments.

Soft robotics may overcome some of these limitations (7–15). Still, while robotic systems with a single soft body are able to achieve highly variable and adaptive behaviors (16), the inherent need to model materials in the large deformation limit makes the design difficult. Furthermore, inspired by flocking observed in nature (17, 18), multi-agent swarm approaches have been successful in generating autonomous, as well as resilient robotic systems by using a large

number of individual robotic units where large-scale collective behaviors emerge through local rules between neighboring units (19–23). Such non-centralized control is able to absorb local perturbations in the inherent noise of the collective organization, and the failure of a few in a swarm of similar units does not necessarily affect the capabilities at the collective scale (23, 24). However, robotic swarms have so far been limited to low density, fluid-like systems with very little overall rigidity of the system as a whole.

The system described in this paper, Granulobots, combines several desirable features of modular, soft, and multi-agent swarm robotics and add unique new capabilities. The Granulobot design is inspired by the highly strain-adaptive behavior of granular matter, as well as its ability to transform between rigid and fluid-like states via a jamming transition (25). The remarkable features of granular matter arise from collective effects in assemblies made of simple building blocks and depend on inter-particles contact properties. Going beyond granular, jamming-based granular actuator systems (7, 26–31) and gear-based metamaterials (32–34) by replacing passive grains with motorized particles adds new options for locomotion (35–39). In granular systems, overall malleable behavior can be achieved even with individually rigid sub-units by designing loose and detachable coupling (36). With the Granulobots, we introduce a novel coupling design that enables continuous deformations and dynamical coupling in aggregates of motorized units. In dense assemblies of multiple Granulobots, this allows for both solid- and liquid-like collective behaviors under a gravity field, which then can be exploited for a range of locomotion strategies. The result is a new form of active granular material that can, at the same time, form the building blocks of a soft robot.

A swarm of Granulobot units, each with a single actuated degree of freedom that enables it to roll like a wheel on the ground, can self-assemble into larger granular aggregates (see Fig. 1A). Units can then shift their positions simultaneously to generate arbitrary overall shapes. An individual Granulobot unit consists of a cylindrical body with an embedded control cir-

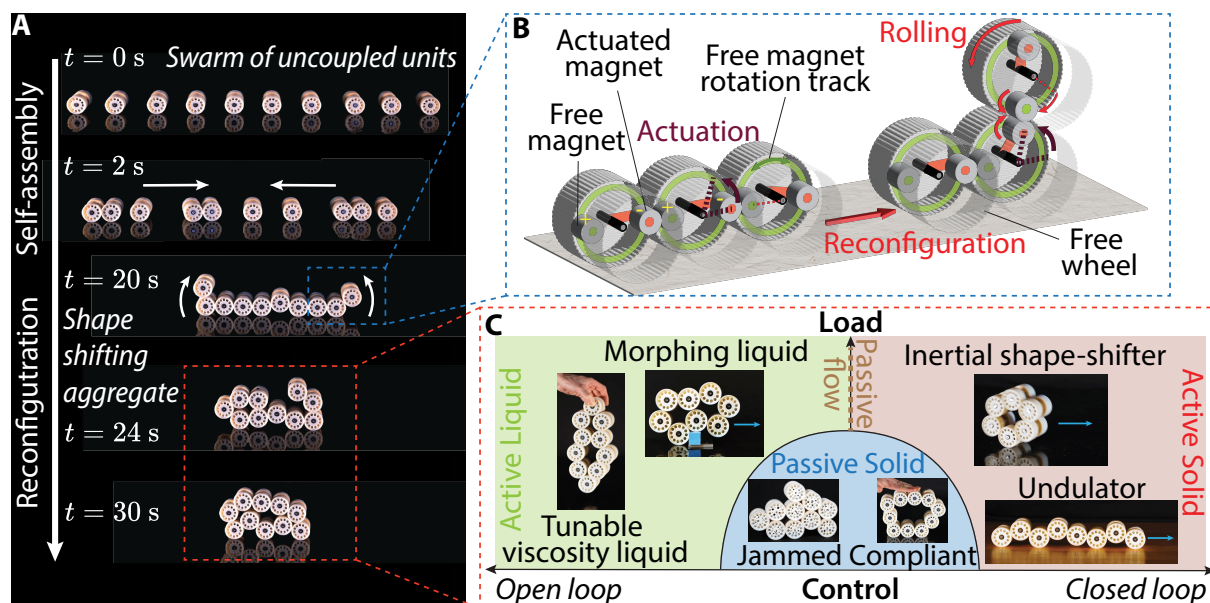


Figure 1: Granulobots: A modular platform bridging soft robotics and active granular materials. See Movie S1. (A) Time-lapse of a swarm of Granulobot units self-assembling into an aggregate and then reconfiguring. (B) Coupling and actuation mechanism inside the Granulobot units. Each two-wheeled unit uses magnetic coupling to connect to its neighbors. Inside a given unit, a single, rotary degree of freedom can be activated to generate torque, which enables this unit to roll along the frictional contact with its neighbor. (C) Granulobot aggregate behaviors, ranging from active liquid to active solid, depending on the type of control. Controlling in open-loop enables behaviors resembling an active liquid with tunable viscosity and the ability to move and morph. In closed loop individual units employ local, onboard feedback and the aggregate can exhibit a range of solid-like behaviors with locomotion gaits that include collective rolling and synchronized undulation. For small applied mechanical loads and sufficiently small bias voltages to the units, friction maintains the aggregate in a passive state that can resemble jammed granular matter or an elastic solid, depending on the units' spatial arrangement.

cuit and two permanent magnets that can rotate about the cylinder’s axis. One magnet rotates freely, while the other one is actuated with a motor. This design allows individual units to move autonomously, mechanically connect with neighbors via magnets, form a continuously deformable aggregate, and apply torque to a neighbor (Fig. 1B). The aggregate’s ability to reorganize its global torque state dynamically allows for collective shape-shifting into the vertical plane and against gravity.

Two modes of controlling the behavior of individual units provide access to a rich set of aggregate behaviors, with responses ranging from rigid and solid to viscous and liquid-like (Fig. 1C). With feedback control, onboard sensors help each Granulobot unit maintain the angular position of its actuated rotor, which leads to a solid-like, i.e., stiff elastic, response of the aggregate. Feedback control can also be used to generate spontaneous, self-organized oscillations. This makes it possible to implement locomotion strategies based on collective rolling or rhythmic undulation (40–42). In contrast, when employing open loop control, the angular position of the rotors is not maintained, allowing for irreversible deformation of the aggregate in response to mechanical load. This can be exploited to create a wide range of fluid-like behaviors of the aggregate, including locomotion, that cause the robot to act like a soft system that yields and conforms to external forces. Importantly, without applied power, a state with structural resistance can be maintained due to a static friction threshold. This is in contrast to other state-changing materials such as electro- and magnetorheological fluids that require large power consumption to maintain a rigid state, which limits their use in autonomous robotics (43).

Results

Granulobot Design Principle

An individual Granulobot unit is itself an autonomous robot, cylindrical in shape with an internal actuator that controls a single rotary degree of freedom. It can magnetically couple to two

other units to form more complex aggregates that can change their shape (Fig. 1A). The actuator, a brushed DC motor, rotates a permanent magnet around a central axis as shown in Fig. 1B (actuated magnet, AM). A second permanent magnet is attached to a passive, freely rotating shaft (free magnet, FM) that can move at the same fixed radius around the cylinder's central axis. When units come into close proximity, the magnetic attraction couples an actuated magnet with a fixed magnet, which allows the units to transmit torque between themselves. When the motor drives the actuated magnet to rotate (brown arrow in Fig. 1B), the magnetic coupling forces the free magnet to follow by rotating around the robot central axis. Since Granulobots are designed with frictional, smooth gear-like surfaces, the produced torques can thus be transferred from the neighbor's free magnet to its robot body. This results in one unit rotating around the other (red arrow in Fig. 1B).

The actuated magnet also acts as an eccentric weight that, when rotated, causes an isolated Granulobot to roll in order to compensate for the shift in its center of gravity. This enables locomotion of individual units and makes it possible for them to assemble into an aggregate once they come within the range of the magnetic coupling force (Fig. 1A). Docking is ensured by using opposite polarities for the magnets. Two possibilities arise: either both magnets have the same polarity in a given unit, in which case units with one polarity dock with units of the other polarity, or all units are identical with one polarity for the actuated magnet and the opposite polarity for the free magnet as shown in Fig. 1B. All results presented here are valid for both cases. Since the free magnet is not attached to any other structure it slides freely along a circular track. Although we limit the present study to a connectivity of two units, i.e. each unit is magnetically coupled to no more than two neighbors, in principle this design allows to add more free magnets for more complex aggregate configurations.

Once aggregates are formed, the system is able to reconfigure and control its behaviors using decentralized algorithms enabled through robot-robot interactions. Each Granulobot contains a

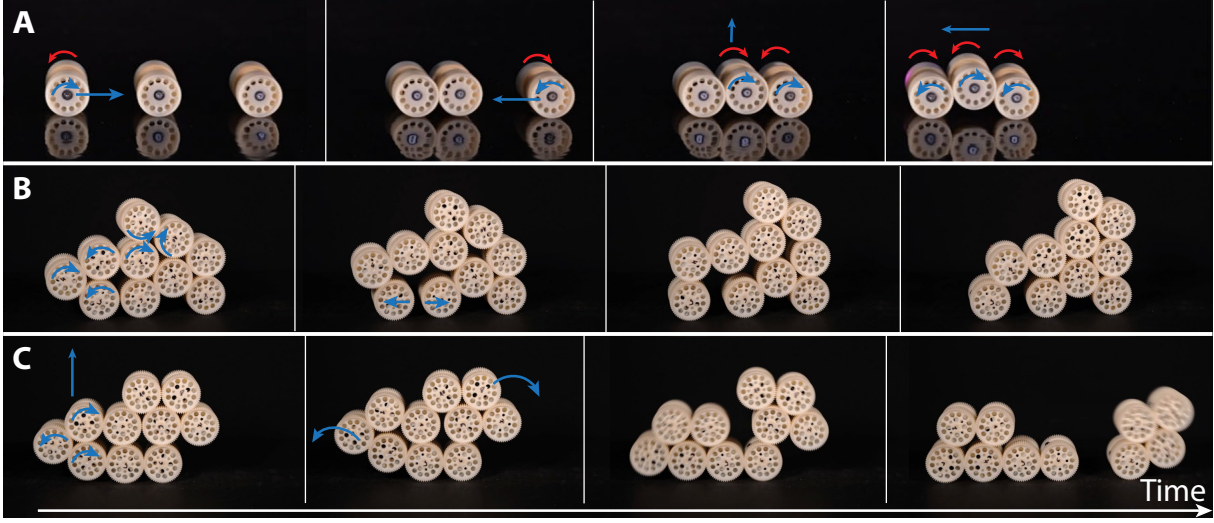


Figure 2: **Self-assembly, shape-shifting and dynamic reconfiguration.** Red arrows represent the actuated magnets' direction of rotation. Blue arrows represent Granulobots in the process of reconfiguration. (A) Individual Granulobot units can roll and attach magnetically into larger assemblies, which then can move using a subset of units as wheels. (B) Exerting torque onto their neighbors, individual units as well as groups of units can reposition themselves and thus rearrange the shape of the assembly. (C) By exerting torque larger than the magnetic binding between neighbors, units can split off and form autonomous robots on their own (See Movie S1).

battery-powered circuit with Wi-Fi capabilities (see Materials and Methods) that can be used for real-time robot-robot communication. For the work discussed here, Wi-Fi communication with a central computer is only used to gather data for post-analysis and for sending initialization commands to all robots. Decentralized locomotion strategies are implemented autonomously by the units via their interactions.

Control of Individual Units and Aggregate Formation / Disassembly

In each individual Granulobot unit i , torque balance with respect to its actuated rotor leads to the following relation among the rotor's angular speed $\dot{\theta}_i$; the torque $\Gamma_{l,i}$ produced by an external load (e.g., from a neighboring unit); the voltage U_i applied to the motor, which produces a torque kU_i ; and the frictional torque from the motor's moving parts, which resists rotation and

has magnitude $\Gamma_f > 0$ (taken to be the same for all units)

$$\eta_0 \dot{\theta}_i = \begin{cases} 0 & |\Gamma_{1,i} + kU_i| \leq \Gamma_f \\ \Gamma_{1,i} + kU_i - \Gamma_f \text{sgn}(\dot{\theta}_i) & |\Gamma_{1,i} + kU_i| > \Gamma_f \end{cases} \quad (1)$$

where $\eta_0 \dot{\theta}_i$ is the torque produced by the motor's back Electro-Motive Force (EMF) and $k > 0$ and $\eta_0 > 0$ are parameters characterizing the motor's load response (see Materials and Methods for the derivation of Eq. 1 and the sign convention for the torques).

As long as $|\Gamma_{1,i} + kU_i| < \Gamma_f$, a Granulobot is effectively in a passive state and does not move. For initially unconnected units in a swarm with $\Gamma_l = 0$, a voltage $U_i \geq \Gamma_f/k$ is required to start autonomous rolling motion and link up with other units. Once the units have self-assembled, a change in the torque that a given unit exerts with its active rotor on its neighbor can lead the whole assembly to reorganize. As soon as an aggregate comprises three or more units, shape-shifting can enable collective locomotion. For example, in the right image of Fig. 2A, the middle unit has lifted off the ground, which allows the aggregate to move (here to the left) by having all wheels that touch the ground rotate in the same direction.

In larger aggregates, applying torque can physically move units on top of others and deform the assembly into an arbitrary configuration within the vertical plane (Fig. 2B). At the points where units contact each other, magnetic attraction provides a normal force strong enough to ensure no-slip gear-like coupling, while units that touch in the absence of magnetic attraction can slide as long as forces exceed the static friction arising from the units' smooth gear surface. These two frictional behaviors prevent units from seizing when three consecutive units come to contact in dense packings.

During such reconfiguration, geometrical constraints that prevent a unit from rotating about its neighbor's central axis can still arise. If further rotation is nevertheless forced and the actuation torque applied becomes stronger than the magnetic coupling, the actuated magnet will separate from its counterpart in the neighboring unit. An ability for individual units to detach

thus emerges from the collective properties of the assembly, without the use of any additional actuator. This allows the reorganization of neighbors in aggregates, and the creation of separate entities that can function as autonomous robots (Fig. 2C).

Choosing a functional form for the voltage U_i in Eq. 1 makes it possible to generate different behaviors for the individual Granulobot units and therefore to design a rich set of collective mechanical behaviors for the aggregate. In the following, we use a general form for each unit i that combines constant torque and position control, by setting a voltage bias u_i and by monitoring the angular position θ_i data from an encoder embedded in each unit's circuitry:

$$U_i = u_i - \left(\alpha \eta_0 \dot{\theta}_i + G \theta_i \right). \quad (2)$$

The parameters $G > 0$ and $\alpha \eta_0$, with $\alpha \in [-1, \infty[$, determine how the drive voltage responds to changes in the rotor's movement, and can be thought of as the coefficients of a proportional-derivative (PD) feedback loop (K_p and K_d , respectively). Using such active control, a unit's electro-mechanical behavior for $|\Gamma_{1,i} + kU_i| \geq \Gamma_f$ in Eq. 1, i.e., beyond the passive state, is then described by

$$ku_i + \Gamma_{1,i} - \Gamma_f \text{sgn}(\dot{\theta}_i) = (1 + \alpha) \eta_0 \dot{\theta}_i + G \theta_i. \quad (3)$$

Here G tunes the Granulobot's ability to maintain its rotor at a targeted position under load, thus acting analogous to a torsion spring constant, while $(1 + \alpha) \eta_0$ tunes the rotor's damping, analogous to viscous dissipation: $\alpha > 0$ increases the damping generated by the back emf $\eta_0 \dot{\theta}_i$, while $\alpha = -1$ actively cancels it. In practice, α is set to values larger than -1 to prevent unstable, divergent behaviors. ku_i corresponds to a torque bias produced by the motor.

Within this framework, driving Granulobots in 'open loop' in Fig. 1C corresponds to setting parameters $\alpha = G = 0$, i.e., ignoring onboard sensor information about θ and $\dot{\theta}$ and controlling the system only via the bias voltages u_i , while 'closed loop' refers to $\alpha \geq -1$ and $G > 0$ so

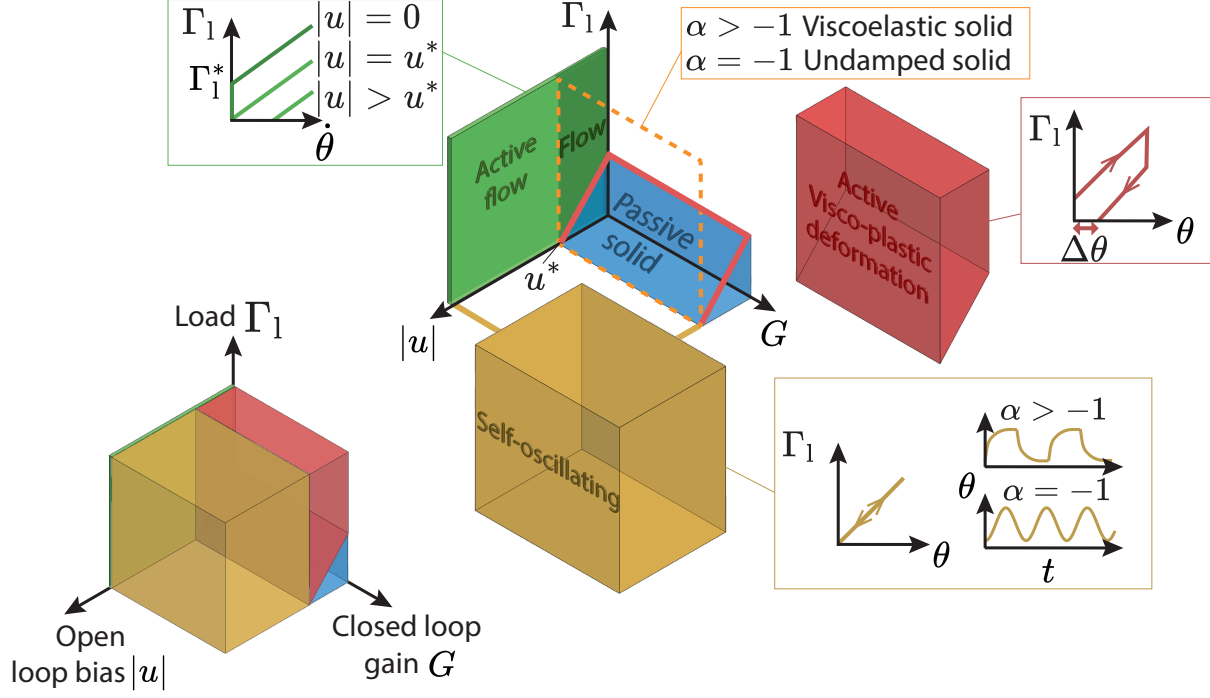


Figure 3: **Dynamical States of a Granulobot Aggregate.** Different states a Granulobot aggregate can exhibit as a function of open loop voltage bias $|u|$, closed loop proportional gain G , and applied torque load Γ_1 (lower left). The exploded view (center) shows in more detail the parameter dependence of the different states, with diagrams indicating the associated load responses.

that the sensor data informs the response. In the next section, we describe how choices for these parameters control the aggregate behavior indicated in Fig. 1C. In a subsequent section we then demonstrate how collective states can be leveraged for different aggregate locomotion control strategies that can be used in different environmental conditions.

Granulobot Aggregate Behavior

Figure 3 sketches the different states of a Granulobot aggregate as a function of applied torque load Γ_1 to the aggregate and two of the control parameters, the voltage bias magnitude $|u|$ and the gain G of the feedback for the angular rotor position. The dissipation parameter α scales the effective viscosity in the liquid state and the relaxation time in the solid state of the aggregate,

but for $\alpha > -1$ does not change the behavior qualitatively. In Fig. 3, all units are driven with a voltage bias u_i of the same magnitude $|u|$ and experience the same average torque load of magnitude Γ_l (of course the sign of these quantities can vary from unit to unit).

Passive State.

If all biases $u_i = |u|$ are sufficiently small, the aggregate remains static until the frictional torque Γ_f in a unit can be overcome. This is the passive state, shaded blue in Fig. 3. When contacts among the units in the aggregate involve only magnetic linkages, the passive aggregate has some degree of elasticity reflecting the stiffness of the magnetic coupling. When both magnetic and nonmagnetic contacts are involved, as in densely packed configurations where a given unit can also be in frictional contact by touching other units, this can create geometric constraints and lead to a granular jammed state with potentially very little elastic behavior (Fig 1C). Such jammed state's response to load will depend strongly on the specific overall configuration of units within the aggregate.

In the following, to simplify the presentation, we consider aggregates where all non-magnetic contacts slip easily and their contribution to friction can be neglected. In this case, the boundaries of the passive state in Fig. 3 are defined by the weakest coupling between units in the aggregate, which corresponds to Granulobots where the bias u_i has the same sign as the load, thus effectively reducing the frictional resistance. This leads to a yield torque $\Gamma_l^* = \Gamma_f - k|u|$, which vanishes once $|u|$ exceeds $u^* = \Gamma_f/k$, and gives rise to the wedge shape of the passive state in Fig. 3.

Liquid-Like States.

These states occupy the green $(|u|, \Gamma_l)$ plane in Fig. 3, where $G = 0$. The bias voltage u^* delineates behavior akin to a yield stress fluid for $u < u^*$ and corresponding to an active fluid for $u > u^*$. For a highly deformable, steady liquid-like load response to emerge, neighboring magnetically coupled units ideally all need to rotate in opposite directions. In an aggregate

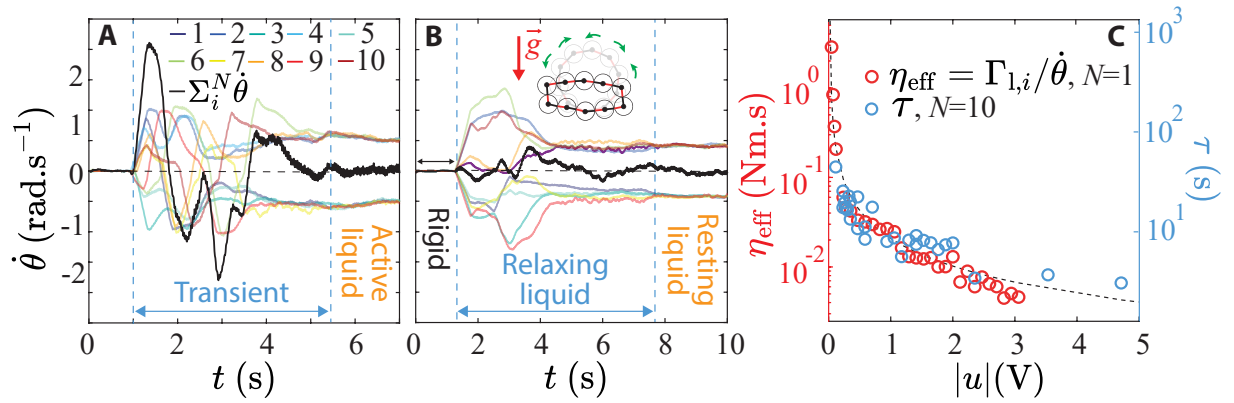


Figure 4: **Active Liquid-like state in a closed-chain aggregate.** $N = 10$ units with $|u| > u^*$, $\alpha = 0$ and $G = 0$. (A) Rotation speeds of individual units as a function of time for an aggregate placed horizontally with $u_i = |u|\text{sgn}(\dot{\theta})$. Here $|u| = 1$ V. (B) Rotation speed of individual units as a function of time during a vertical collapse experiment with $|u| = 1$ V. (C) Red circles: Evolution of a unit's damping parameter $\eta_{\text{eff}} = \Gamma_{1,i}/\dot{\theta}_i = \eta_0 + k(u^* - |u|)\dot{\theta}_i^{-1}$, evaluated from measurements of $\dot{\theta}_i$ on a single unit, as a function of voltage bias $|u|$, for a typical load $\Gamma_{1,i} = mgr = 0.024$ Nm, where m is the unit's mass, r its radius and g the acceleration of gravity. Blue Circle: Evolution of the relaxation time scale τ , measured for the collapsing chain, as a function of voltage bias $|u|$. Dotted line: η_{eff} evaluated using the analytical form of $\dot{\theta}_i$ obtained from Eq. 3 (see Methods), and for a typical load $\Gamma_{1,i} = mgr$.

comprising a closed chain of an even number of units N , this translates into $\sum_i^N \dot{\theta}_i \approx 0$. Such regime is reached autonomously by setting $u_i = |u| \text{sgn}(\dot{\theta}_i)$ in each of the individual units (in this case onboard sensing of the rotor's direction of rotation is required). The mechanical coupling then drives a self-organization process that, after a brief transient regime, converges to a state with bias voltages of opposite sign on neighboring units, $u_i = -u_{i-1} = (-1)^i |u|$ (Fig. 4A, Movie S2 part 1). Alternatively, the liquid state can be achieved in fully open loop, with no sensing of $\text{sgn}(\dot{\theta}_i)$, by initializing neighboring units via a global command to use $|u|$ of opposite signs (See Methods), and with $\alpha = 0$. From Eq. 3, for $G = 0$ the load response of all individual units, and thus for the aggregate, is described by an equation of the form

$$\Gamma_{1,i} = (1 + \alpha)\eta_0\dot{\theta}_i + k(u^* - |u|), \quad (4)$$

written here for positive $\Gamma_{1,i}$ and therefore $\dot{\theta}_i > 0$ and $\text{sgn}(\dot{\theta}_i) = 1$.

If $|u| < u^*$, this relationship between applied load and resulting rotation speed has the same functional form as the relationship between applied stress and shear rate for a yield stress fluid (see sketch of $\Gamma_1(\dot{\theta})$ in Fig. 3). For such fluid an effective, rate-dependent viscosity η_{eff} is defined by the ratio of stress to shear rate. By analogy we here define a unit's viscous damping as $\eta_{\text{eff}} = \Gamma_{1,i}/\dot{\theta}_i$.

To compare this with the viscous behavior of a multi-unit Granulobot aggregate in its liquid state, we characterize the collective viscous flow by performing experiments where we time the collapse of a circular chain units (Fig. 4B, Movie S2 part 2). Before the collapse $u = 0$, the load on all units is below their yield torque, and the chain's circular shape is maintained. We then switch on the bias $|u|$ to drive the system into the liquid state and measure the relaxation time τ needed for the aggregate to reach its minimum potential energy, i.e., its equilibrium state. To bypass the transient phase of the self-organizing process and ensure the system behaves as a liquid as soon as the voltage bias is applied, we enforce $u_i = (-1)^i |u|$. Note how

adjacent units rotate in opposite directions and how this complex sequence of interdependent rotations emerges simply in response to external forcing. As such, it can accommodate arbitrary starting configurations and will always proceed in a liquid-like manner toward the equilibrium configuration that minimizes gravitational potential energy.

Figure 4C shows measurements of η_{eff} (red circles) and τ (blue circles) as a function of the voltage bias $|u|$. The plotted η_{eff} is for an individual unit, obtained by applying a fixed torque $\Gamma_{1,i}$ less than the yield torque, measuring the resulting angular speed $\dot{\theta}$ as a function of $|u|$, and using Eq. 4 to obtain $\eta_{\text{eff}} = \Gamma_{1,i}/\dot{\theta}_i$. We observe that τ reproduces this behavior of η_{eff} , consistent with a collective viscosity that scales with bias $|u|$ in the same way as η_{eff} . This demonstrates how the collective viscosity can be tuned by setting the viscous load response of the individual units. Key to this tuning is the bias $|u|$, while changing the damping via α , which is set to zero in all the data shown in this section, only scales the behavior via a prefactor (44). For vanishing voltage bias $|u|$ the passive state is approached and η_{eff} diverges.

Conversely, as $|u|$ is increased to the point that it reaches u^* , the yield stress vanishes and the viscosity attains a load-independent value $(1 + \alpha)\eta_0$. Effectively, the system now behaves like a Newtonian liquid. Finally, if $|u|$ is increased above u^* , individual units rotate with finite $\dot{\theta}_i = \frac{k(|u|-u^*)}{(1+\alpha)\eta_0}$ already in the absence of any significant load (see e.g. the final equilibrium state in Fig. 4B). In this state the aggregate behaves in a manner that can be characterized as an active liquid with low effective viscosity.

Solid-Like States.

These states use a feedback to sense the rotor movement and drives it toward its equilibrium angular position during a load perturbation. They are shaded red and orange in Fig. 3. With increasing G , the response of individual units, and thus also of the aggregate, becomes more elastic and rigid.

Considering a bias that acts against the frictional torques $u_i = |u| \text{sgn}(\dot{\theta}_i)$, Equation 3 can

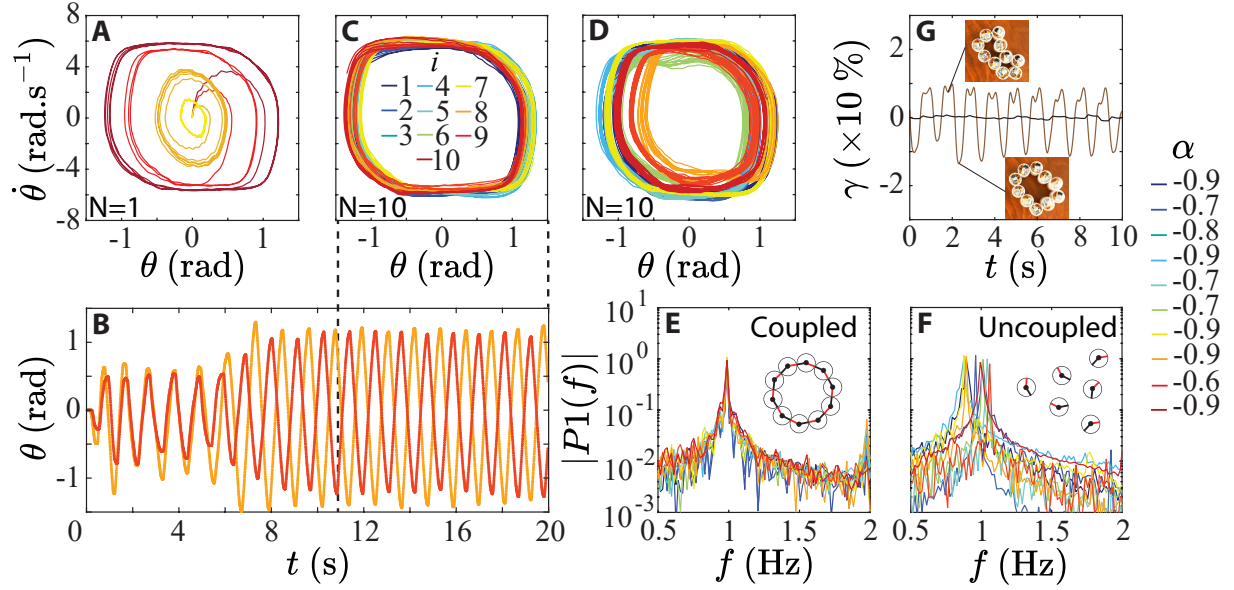


Figure 5: **Self-oscillating solid-like state in a closed-chain aggregate.** Granulobots are laid horizontally onto a slippery surface, $|u| > u^*$ and $G = 1.0$ Nm/rad. (A) Phase space $(\theta, \dot{\theta})$ of a single isolated unit for different $|u|$ and α . $|u| = 2$ V, $\alpha = -0.9$ (brown); $|u| = 1$ V, $\alpha = -0.9$ (red); $|u| = 1$ V, $\alpha = -0.5$ (orange); $|u| = 1$ V, $\alpha = 0$ (yellow). (B-G) $N = 10$ units. (B) Angle as a function of time for two coupled neighboring units in the chain aggregate, after turning all units on at $t = 0$. $|u| = 1.0$ V. (C) Limit cycles followed by all coupled units in the steady regime of the experiments corresponding to (B). (D) Limit cycles observed in an aggregate with α in the range $[-0.9, -0.6]$ and $|u| = 1.0$ V. (E,F) Amplitude frequency spectrum observed for each of the units when coupled into a ring aggregate (E) and when isolated (F). (G) Shape deformation $\gamma = (A - A(t = 0))/A(t = 0)$ as a function of time, with A the area covered by the assembly, for an aggregate with $\alpha_i = \alpha$ as in (B,C) (black), and with a range of α as in (D,E) (brown curve).

be written as

$$\Gamma_{1,i} = G\theta + (1 + \alpha)\eta_0\dot{\theta}_i + k(u^* - |u|), \quad (5)$$

When $|u| < u^*$, this behavior is analogous to a viscoplastic solid, which corresponds to the response of a spring, a damper and a frictional element in parallel (45). In this regime, the characteristic response time of a rotor is $\tau = (1 + \alpha)\eta_0/G$. As the biases will not completely cancel the frictional torques in individual units, deformation will exhibit some hysteresis $\Delta\theta = k(u^* - |u|)/G$. The overall aggregate will then respond to load with some plasticity.

For effective position control, a fast response with negligible hysteresis is achieved by choosing a positive α and a large G . If $\alpha = -1$, all damping is actively compensated for and a perturbation of the rotor that overcomes Γ_f leads to steady undamped oscillations. When $|u| = u^*$ (vertical dotted plane in Fig. 3), Equation 3 correspond to a viscoelastic solid, the response of a damper and a spring in parallel, and the hysteresis disappears. Vanishing damping $\alpha = -1$ then corresponds to an undamped mass-spring oscillator.

If we choose biases $|u_i| > u^*$, the rotor is forced away from its equilibrium angle and oscillations arise spontaneously, even without applied load. Each unit is then driven by the bias to "self-oscillate" such that they exhibit well defined limit cycles with amplitude and frequency fixed by $|u|$, G and α (Fig. 5A). When units are coupled together, they can transfer momentum to each other via their spring-like oscillation, and thus perturb their dynamical state. In a chain of units, after an initial transient, this coupling can lead to the self-organization of collective oscillatory states with well defined limit cycles that remain unchanged over time. Specifically, in a closed loop of an even number of units that all have the same parameters, we observe a synchronization process. Figure 5B displays such situation in an aggregate of $N = 10$ units, by showing the angles of two consecutive units as a function of time, right after turning them on. After a transient, units lock in their phase and amplitude (see Movie S3 part 1). The frequency and amplitude observed in the aggregate are the same as for an isolated unit (Fig. 5C).

Remarkably, the system self-organizes such that consecutive units' phases alternate between 0 and π , which corresponds to $\dot{\theta}_i = -\dot{\theta}_{i+1}$, and $\sum_i^N \dot{\theta}_i \sim 0$. In this situation, the contour of the chain remains static in time with no deformation. We label this collective steady state a self-oscillating solid. A similar phenomenology is observed when choosing u_i across all units with the same sign, regardless of Γ_f (46).

When units have different parameters and thus individually exhibit different oscillation frequencies, we still observe collective limit cycles characterized by self-organization with frequency and phase locking. Figure 5D shows such collective limit cycles for an assembly with a distribution of α in the range $[-0.9, -0.6]$. Figures 5(E,F) compare the frequency spectra of each unit in a coupled aggregate with those for isolated units. We see that the mechanical coupling selects a single collective frequency despite the spread in frequencies of isolated units. At the same time, there remains a spread in oscillation amplitudes (Fig. 5D). To accommodate this, the chain shifts the units' phases (see Supplementary Material) and deforms globally (see Movie S3 part 2). Figure 5G shows the evolution of such deformation as a function of time for an assembly with fixed α (same as in 5(B,C)) and for the same range of α as in Figure 5(D,E). We observe that when there is a range of α values, the limit cycles are accompanied by a periodic deformation of the aggregate's shape (Movie S3 part 2).

From collective states to decentralized locomotion tasks

The behaviors summed up in Fig. 3 show a wide range of responses to external loads and constraints. Such mechanical feedback from the environment can be seen as an emergent and decentralized collective mechanical sensing ability that can be harnessed for control. These collective states can be driven out of their effective equilibrium to produce dynamical shape shifting solely by preventing individual units behavioral state, enabling deformation based tasks. Furthermore, the use of voltage control via a single functional form (Eq. 2) allows to continuously

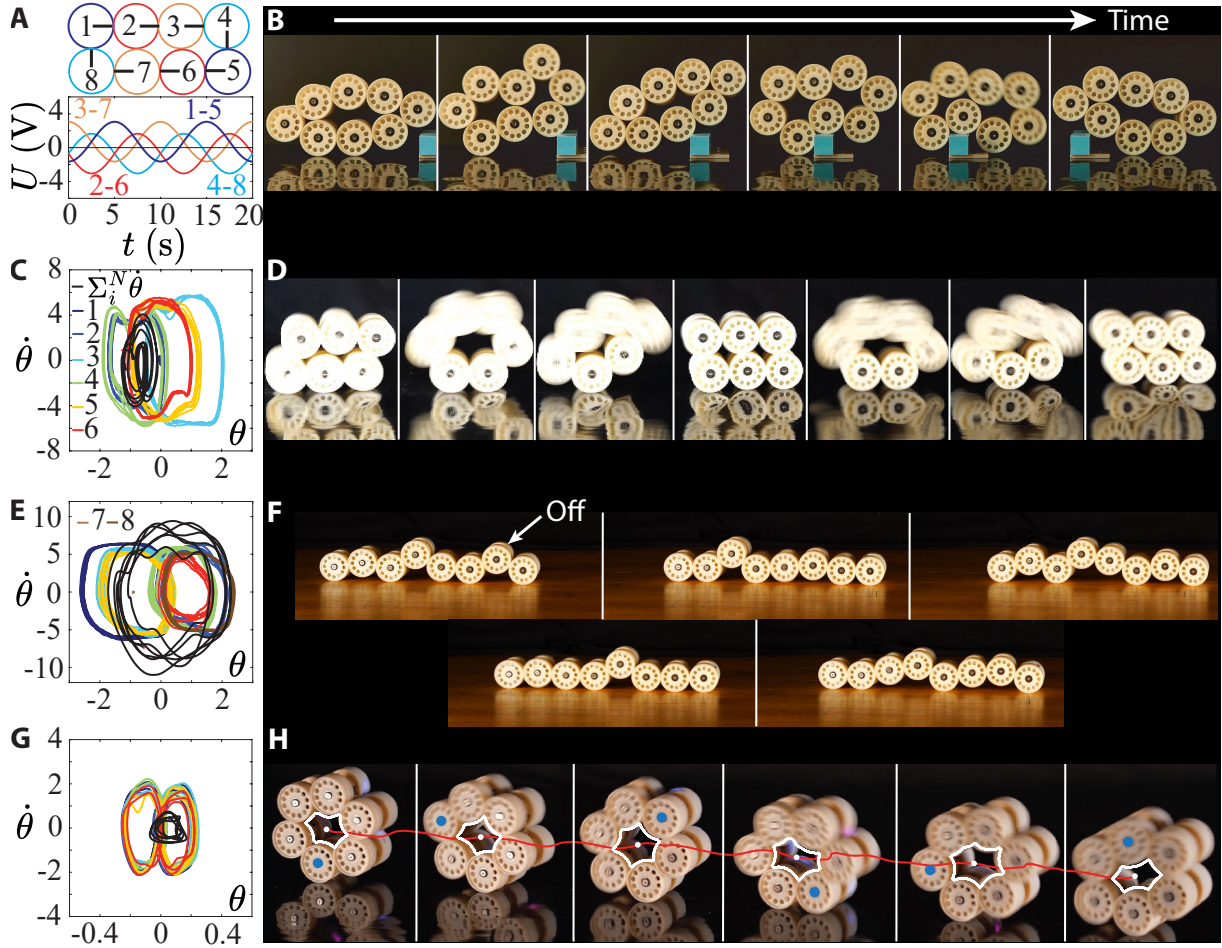


Figure 6: Exemplary Granulobot locomotion strategies. (A) Liquid-like gait using a set of voltage biases with shifted phases in an aggregate of $N = 8$ units (see Materials and Methods, $u_0 = 0.7$ V and $A = 2.4$ V). (B) Snapshots of a Granulobot aggregate using the gait (A) to move over an obstacle. (C) Limit cycle reached by a closed chain aggregate in the self-oscillating solid state with $N = 6$ units, after turning unit $i = 1$ off ($|u| = 2$ V, $\alpha = -0.9$ and $G = 1.0$ nm/rad). (D) Snapshots of a steadily moving self-organized aggregate corresponding to the gait in (C). (E) Limit cycle of an open chain aggregate in the self-oscillating solid state with $N = 8$ units, after turning unit $i = 7$ off ($|u| = 1$ V, $\alpha = -0.9$ and $G = 0.5$ Nm/rad). (F) Snapshots of a steadily moving self-organized aggregate corresponding to the gait in (E). (G) Limit cycle from a leader-follower scheme to implement a propagating perturbation (inertial shape-shifter). Choosing $|u|=0$, $G = 10.0$ Nm/rad and $\alpha = 1.0$, units can be controlled in displacement (large G with $|u| < u^*$), enabling fast collective motion with small deformation by turning into a “pumping” wheel. (H) Snapshots corresponding to gait (G). The blue dot corresponds to unit $i = 1$. In (C), (E) and (G) the units of θ and $\dot{\theta}$ are rad and rad/s, respectively.

transition between states of different response type and switch autonomously between strategies depending on environmental or computation constraints. We demonstrate this ability by implementing three different locomotion gaits. Using the liquid-like, the self-oscillating and the viscoplastic mechanical responses, a robot can move over an obstacle without sensors, self-organize into a steadily translating aggregate solely via mechanical coupling on frictional or slippery surfaces, and can move quickly and efficiently using its own inertia.

Morphing Liquid for Sensorless Obstacle Management. We leverage the aggregate’s ability to change its rigidity and behave as a liquid to locomote over an obstacle, using only mechanical feedback from the environment. For an aggregate to deform liquid-like while translating its center of mass without sensor readout, we must find a form of u_i that implements a gait while satisfying $\sum_i^N \dot{\theta} \sim 0$. Here we show that this can be achieved with $\alpha = G = 0$ by using the functional form for the individual u_i displayed in Fig. 6A, which we have inferred from a reverse kinetic approach (see Materials and Methods). This gait relies on synchronous periodic deformation that we can implement with both closed or open chain configurations (see Materials and Methods), by allowing neighboring units to wirelessly synch their clocks and correct phase drift over time. Figure 5B shows a snapshot of an aggregate “flowing” over an obstacle to pass it (see Movie S1).

Undulator: Emergent aggregate gait with coupled oscillators. Figure 5G shows that a spread in the units’ oscillation properties in an aggregate leads to limit cycles that generate periodic collective shape deformations. Even when there is no spread, similar collective shape deformations can be triggered by mechanical interaction with the environment. Specifically, when an aggregate of units, all with equal control parameters, is placed vertically onto a non-slip surface, limit cycles are still reached and small regular left-right periodic deformations emerge due to frictional constraints: units that are in contact with the non-slip surface cannot rotate as much as the others. In such setting, perturbing this state further by turning off one

unit modifies the limit cycle (Fig. 6C), breaks the left-right symmetry of the collective periodic deformation, and amplifies it. This can lead to a sustained locomotion of the aggregate (Fig. 6D) without the use of wireless communication, solely relying on unit-unit mechanical interactions, and hence minimal computation (See Movie S3 part 3). To locomote with a closed chain, the left-right symmetry of the periodic deformation can also be broken by using an odd number of units with identical oscillation parameters (see Movie S1). In an open chain configuration, periodic deformation can be used to locomote on a slippery surface. In that case, perturbing the properties of an oscillator in one portion of the chain can trigger an undulating deformation that changes the contact with ground periodically between different sections of the chain (Fig. 6(E,F), Movie S1).

Inertial Shape-Shifter. Here we demonstrate the implementation of a local displacement control approach that generates efficient locomotion via rolling an aggregate in its solid-like state. This is achieved via fast and overdamped local feedback loops in the viscoplastic region of Fig. 3, with large G , $|u| = 0$ and an optimal α . Small, appropriately timed shape perturbations are propagated through a ring-like, rigid chain of coupled units to generate coordinated locomotion that leverages the assembly’s overall inertia. The shape perturbations are enforced by controlling the rotors’ absolute angles as a function of time (see Methods for details). The aggregate’s locomotion is triggered in a decentralized way by sending the same message once to all units. Neighbor-neighbor communication and a leader-follower algorithm then implement a predefined angle perturbation that propagates through the chain. Depending on the algorithm parameters, the aggregate can either crawl or roll, the latter demonstrating the faster and most energy efficient locomotion strategy as only small rotor displacements are required (Fig. 6(E,F) and Movie S1).

Conclusions

The Granulobot represents a novel robotic system inspired by granular material where motorized units can flexibly and reversibly couple with each other and self-assemble into larger aggregates. A minimal design with a single activated degree of freedom per unit enables aggregates to reconfigure dynamically and to transition between solid- and liquid-like responses under gravity. In contrast with modular robotic systems that require successive steps of detachment and reattachment of individual units to change their shape, a Granulobot aggregate can deform by continuous local displacement, similar to a deforming soft material. Since such deformation is a function of the Granulobot’s dynamical state, this results in the wide range of collective mechanical behaviors shown in Fig. 3. Furthermore, as the different behaviors are all encoded in the functional form of the control voltage U_i , this allows to transition continuously between liquid-like behavior associated with open loop control, and solid-like behavior where an onboard feedback loop monitors the local rotor displacement sensor.

The properties associated with several of the Granulobot aggregate states make it possible to use mechanical interaction with the environment to implement decentralized locomotion strategies without the use of electronic environmental sensing and at minimal computation cost. In the liquid-like state, this allows an aggregate to pass over an obstacle by “flowing” over it. In the self-oscillating solid state, Granulobots self-organize strictly via mechanical coupling into well-defined limit cycles. In this setting, changes in the control parameters, as well as in the mechanical environment where robots operates in, can trigger periodic deformations. Using this feature, an open chain can rhythmically deform and slide on a slippery surface, and a closed chain can periodically morph to move on a no-slip surface. We find that the existence of these frequency locking states is robust to noise and perturbation. Furthermore, transitions toward self-organized states exhibit a strong hysteretic behavior, with long transient regimes at biases

close to u^* , and almost instantaneous transitions at large biases. Similar to subcritical behaviors in other dynamical systems, this means that states can be switched from a disordered state to a well-defined self-organized one via an external perturbation, with a sensitivity that can be tuned with the voltage bias. Such property enables adaptivity to the environment without requiring electronic feedback.

The viscoplastic state makes it possible to maintain an aggregate shape and exhibits less sensitivity to perturbation compared to the self-oscillating state. This state is more amenable to implementing traditional displacement control, where parameters can be tuned for a rigid response that is insensitive to external environmental loading, similar to control of a robotic arm. In our experiments with closed chain aggregates, this is advantageous when implementing locomotion that uses inertia. It also demonstrates the ability of the design to combine in a decentralized way our physical approach with more widely used kinematic planned strategies. This is also the regime in which controlled neighbor reconfiguration can be implemented, in a usage more similar to existing modular robotic system. But such reconfiguration can happen spontaneously in any of the accessible states through collective mechanisms.

We view the different locomotion strategies explored here as first examples that demonstrate the versatility of the Granulobot platform. As such, we anticipate that many additional locomotion strategies could be found, as well as new tasks possible. A promising way to explore them could be to implement machine learning approaches such as in (47, 48). A more ambitious but crucial step would be to implement learning in a fully decentralized way, which could allow aggregates to select autonomously strategies that are relevant to the environment and constraints they encounter. In this context, conventional machine learning approaches are conceptually challenging to apply since error functions are ultimately estimated centrally. We believe that the Granulobot platform offers a promising perspective for tackling this problem by combining the collective behavior emerging from mechanical interactions among the units with

local error optimization executed in the units' microcontrollers.

Furthermore, more complex packing and coupling structures could be created by increasing each unit's connectivity with additional passive magnets and, in dense packing configurations, exploiting the metastability associated with granular jamming. For instance, it should be possible to maintain structural rigidity at no energy cost, and switch configurations by actuating only few units where resistance to reconfiguration is weaker (25). Additionally, larger connectivities would increase the effect of couplings and could allow for more collective mechanical adaptability (51). Finally, while the Granulobot aggregates discussed in this work are effectively two-dimensional, arranging two or more units horizontally next to each other and flexibly coupling them suggests a straightforward extension to a 3D version, while the simple contact and actuation principle that we propose could be integrated in larger scale programmable matter (5).

Materials and Methods

Robotic prototype

The Granulobot prototype discussed in this work consists of 3D printed parts, permanent magnets, a battery-powered electronic circuit and a geared DC motor (Fig. 6A). Each individual Granulobot unit is comprised of three co-axial components that can rotate independently from each other: (1) a first wheel, which contains the DC motor (N20 from Pololu) that drives a rotor with a magnet at its end; (2) a second rotor, also with a magnet at its end, that can move freely around the central motor axis; and (3) a freely rotating second wheel (shown at the top of the exploded view in Fig. 6A) that helps align the Granulobot units when making contact and stabilizes an assembled aggregate against tipping over. Both rotors hold hollow cylindrical neodymium magnets (N54 from Supermagnetman, size $3 \times 12 \times 15.5 \text{ mm}^3$) via a shaft with ball bearings on each end, which let the magnets rotate freely. The active rotor attaches to the motor shaft with two screws to adjust parallelism. The motor's gear train can be changed

to different ratios β depending on the application, with values ranging from 150:1 to 1000:1. Additional passive rotors could be added to increase the connectivity of a single unit and build more complex aggregate structures if desired.

Individual Granulobot units have an overall width $l = 62$ mm and a wheel diameter $2r = 48$ mm (OD). 3D printed parts are made with a UV-curing polyjet printer (Stratasys J850) using an ABS-like resin (RGD511 and 535) and with a Phrozen Mini 4k printer using Loctite Onyx 410 engineering resin. The total weight of a single Granulobot unit with geared motor, printed circuit board (PCB), ball bearings, magnets, and two 220 mAh batteries is 98 g.

The custom electronic circuitry consists of a Wi-Fi enabled microcontroller (Espressif ESP-32), an H-bridge to control the motor, a power management circuit with 3.3 V and 6 V regulation from two single-cell lithium-ion polymer (Li-po) batteries, a 6-axis linear and gyroscopic accelerometer, a magnetic sensor with sensitivity in the range of the field produced by the rotor magnets, and a continuous magnetic encoder to measure the motor rotation. All electronic components are assembled on a printed circuit board designed to fit within the circular Granulobot body (see Fig.6B). The motor voltage is produced by two microcontroller digital outputs using pulse width modulation (PWM), averaged out by the low frequency response of the motor system. The entire circuit is controlled and monitored by a firmware coded in C++ with Arduino and Esp32 libraries. Data can be sent and received by Wi-Fi between individual units as well as with an external computer. For the latter, we developed Python software that gathers data for post-analysis and visualisation, at a rate of approximately 200 Hz, and that can execute scripts with a sequence of instructions. This interface also allows to reprogram remotely all robot units simultaneously for firmware changes.

Individual motor behavior

In a DC motor the current I through the winding generates a torque $\Gamma = K_t I$, where the

constant K_t depends on the mechanical and electromagnetic properties of the motor (49). Our sign convention is that positive current I produces positive torque and positive gearbox output rotor speed $\dot{\theta}$ (Fig. 7A). The torque balance in the steady state of a loaded motor can then be expressed as

$$\beta K_t I + \Gamma_l - \Gamma_f \text{sgn}(\dot{\theta}) = 0, \quad (6)$$

where β is the gear box ratio, Γ_l is the external load on the motor's gearbox output, counted positive if it acts along the rotation direction and negative otherwise (Fig. 8A), and $\Gamma_f > 0$ is the magnitude of the friction torque that arises from the mechanical parts contacting each other inside the gearbox and the rotor system. The sign function $\text{sgn}(\dot{\theta}) = \dot{\theta}/|\dot{\theta}|$ appears because the friction torque always opposes any rotation. Using Kirchhoff's law, the motor current I during steady rotation obeys

$$RI = U + E, \quad (7)$$

where R is the motor resistance, U the voltage applied to the motor, and E the back electromotive force (e.m.f.). The latter opposes the motion of the inner rotor, which spins at speed $\omega = \beta\dot{\theta}$, and can be expressed via Faraday's law as $E = -K_e\omega$, with K_e being the e.m.f.

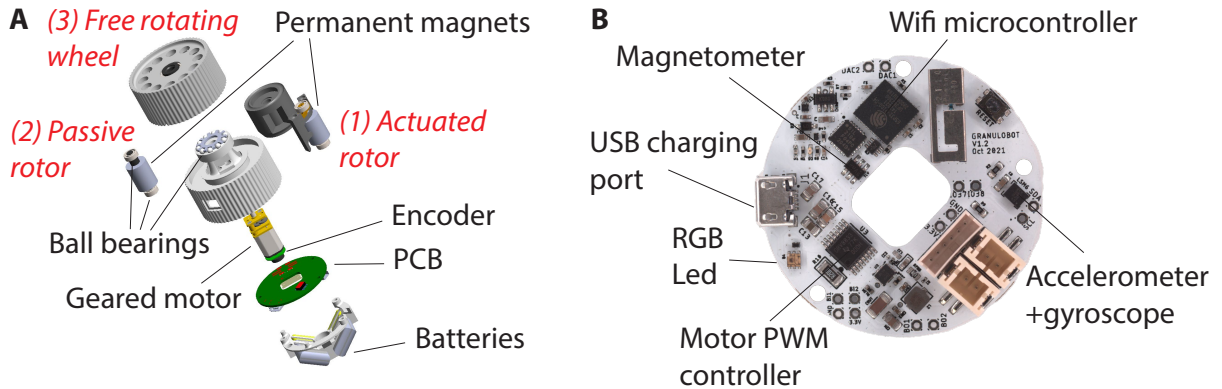


Figure 7: **Granulobot design.** (A) Exploded view of a Granulobot 3D model. (B) Assembled electronic circuitry custom-designed to drive the mechanical hardware.

constant of the motor. Equation 7 combined with Eq. 6 can be rewritten as:

$$\beta \frac{K_t}{R} U + \Gamma_1 - \Gamma_f \text{sgn}(\dot{\theta}) = \frac{K_t K_e}{R} \beta^2 \dot{\theta}. \quad (8)$$

Theoretically $K_t = K_e$, but in practice these two value can be slightly different, and we therefore distinguish them in what follows. Furthermore, K_t tends to decrease with an increasing gear ratio; thus, it is important to estimate it whenever β is changed (see SI for estimates of K_e and K_t). Defining $\eta_0 = \beta^2 K_t K_e / R$ and $k = \beta K_t / R$ we arrive at Eq. 1 in the main text for the case of steady-state rotation, i.e., for the case that $|\Gamma_1 + kU| > \Gamma_f$ where the frictional torque has been exceeded.

From Eq. (8) or, equivalently, Eq. 1 we expect the speed-torque curves to be linear with slope η_0 once the load Γ_1 exceeds the yield threshold torque. When kU becomes larger than $\Gamma_f \text{sgn}(\dot{\theta})$ the yield threshold vanishes, and the units will exhibit rotation already without applied torque, at zero-load rotation speed $\dot{\theta}_0 = \eta_0^{-1}(kU - \Gamma_f \text{sgn}(\dot{\theta}))$.

Figure 8B shows that this is consistent with data from experiments where we systematically

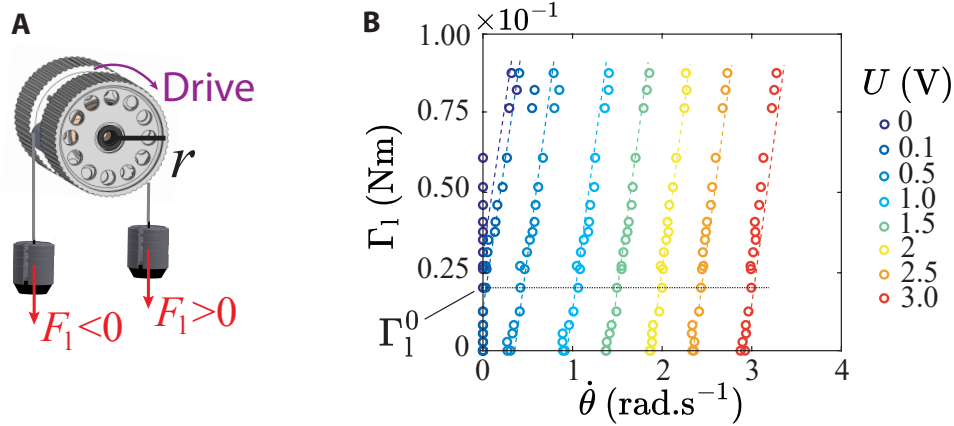


Figure 8: Granulobot motor response to load. (A) The curves represent the torque load as a function of rotation speed for different voltages. The dotted line represent Eq. 8 with $R = 9.6 \, \Omega$, $K_e = 2.65 \times 10^{-3} \, \text{NmA}^{-1}$, $K_t = 5.8 \times 10^{-3} \, \text{NmA}^{-1}$, $\Gamma_f = 0.024 \, \text{Nm}$. K_t and Γ_f are obtained by fitting the data with affine functions and averaging the fit parameters. (B) Positive torque is counted as pointing in the same direction as the rotation speed vector for positive drive. $\beta = 379$.

varied Γ_1 and measured $\dot{\theta}$ for different voltages U controlled by pulse width modulation (PWM; see SI for calibration of PWM parameters). Only very close to zero bias voltage, where the rotor remains at rest until a certain torque load threshold Γ_1^* is exceeded, are there deviations. In particular, for the smallest voltages the angular speed just above Γ_1^* is underestimated by the model.

The parameters R and K_e can be determined for each motor from measurements of the motor current performed simultaneously with the experiments presented in Fig. 8B (see SI). To determine K_t and Γ_f , we fit Eq. 8 with the data in Fig. 8B.

In an aggregate of several units, the local load $\Gamma_{1,i}$ applied to any particular unit i will arise from the magnetic coupling to its neighbors, for example from the weight of units above (similar to hydrostatic pressure) or from externally imposed forces on the aggregate. As a consequence of the frictional torque in each unit, the system can hold its shape like a solid at zero or small voltage as long as the local torque loads never exceed the yield threshold, i.e., up to the point where $|\Gamma_{1,i} + kU_i| > 0$. Otherwise, the rotor will turn under the load and the overall shape will “flow” in a manner analogous to the behavior of a yield-stress fluid. Since each unit’s encoder provides direct access to $\dot{\theta}$, we can use Eq. (8) to extract $\Gamma_{1,i}$ as a function of time from each unit.

Morphing liquid passing an obstacle

The onboard monitoring of the rotor angle in each unit makes it possible to develop suitable locomotion strategies by reverse engineering. This proceeds by manually ‘teaching’ the Granulobot aggregate how to overcome a type of obstacle, recording the potentially complex sequence of local angle changes, and from it extracting the essential features required for successful obstacle management. To do so we follow these three stages:

1. We first put the system in the liquid state, with a low typical damping $\eta_{\text{eff}}^0 < 0.01$ Ns/rad,

which corresponds to $|u_i| = u_0 > 1.5 \text{ V}$, such that it behaves as a passive liquid aggregate. We then deform the aggregate by hand to pass it over an obstacle. Once a continuous sequence of deformations has been successful in overcoming the obstacle, we reproduce by hand the same sequence without obstacle and record via the Wi-Fi data acquisition platform the associated time-dependent angle changes for each Granulobot unit.

2. We “play back” these angle variations from a central computer to each Granulobot, which they follow via local feedback using the rotor encoder. The voltage signals generated by the feedback loops are recorded. We then use these voltages to infer a general, time-dependent voltage bias $u_i(t)$ appropriate to overcome the type of obstacle just trained on. Figure 6A shows an aggregate of eight Granulobot units in a closed chain, trained to ‘flow’ over an obstacle. During training by hand we observe that all eight $u_i(t)$ are oscillating at a similar frequency and amplitude. Furthermore, the signal of a given Granulobot is shifted in phase compared to its neighbor, while Granulobot units placed at opposite positions (i and $i + N/2$) along the chain seem to have the same phase. We generalize this behavior by using a simple periodic function for the bias voltage that shifts each unit’s phase by $4\pi/N$ such that $u_i = (-1)^i u_0 + A \sin(\omega t + \phi_i)$, with $\phi_{i+1} = \phi_i + \frac{4\pi}{N}$ and A the amplitude of the oscillation (shown in Fig. 6A).

3. We send to each Granulobot the address of their neighbor such that they can implement locally the bias u_i defined in step 2 above, with u_0 and A as user-defined parameters.

When using such a control strategy, only the pair of parameters (u_0, A) must be sent. As the peak voltage A is increased, the aggregate becomes more compliant and follows the contour of the obstacle more closely. This is consistent with a smaller effective viscosity.

Inertial shape-shifter

The inertial shape-shifter moves by configuring the Granulobot units into a ring-shaped chain and then applies a suitably chosen shape perturbation that propagates around the ring to drive an overall rolling motion, as shown in Fig. 6(H) and Movie S1. In a closed chain geometry, the sum of angles must satisfy an overall geometric constraint (50), namely $\sum_{i=1}^N \theta_i(t) = \pi(N-2)$. All angle perturbations $[d\theta_1 \dots d\theta_i \dots d\theta_N]$ of units $[1 \dots i \dots N]$ must then satisfy $d\theta_i = \sum_{j \neq i}^{N-1} d\theta_j$. To achieve this kinematic control in a decentralized way, with the same instructions sent to all the Granulobot units, we used a local communication strategy whereby one unit will temporarily become the leader and the others followers. This control strategy can be implemented as a sequence of four sets of instructions that are sent once to all units simultaneously at the initial stage:

1. Learning the initial topological configuration. The sequence of all units' addresses in the ring-like chain is sent, providing units with information about which of their two direct neighbors is the one connected to their active rotor.
2. Kinematic constraints and initial position of the perturbation. An initial leader address and a number of trailing followers are chosen. This leader and its followers then implement a perturbation as follows: The leader sends in real-time to its actuated neighbor the value of its angle θ_i . This value is propagated through all the followers by neighbor-neighbor communication until the last follower is reached. Every follower applies a rotation that is a linear combination of the leader readout $d\theta_{i+1} = \alpha_{i+1} d\theta_i$, such that the full sequence of coefficient $\{\alpha_1, \dots, \alpha_N\}$ satisfies the angle conservation relationship $d\theta_i = \sum_{j \neq i}^{N-1} d\theta_j$.
3. Leader unit perturbation. The angle of the leader unit is perturbed according to $d\theta_i(t) = d\theta_0 \sin(\pi t/T)$, where the parameters T and $d\theta_0$ are chosen to control the shape of the

perturbation.

4. Perturbation propagation. When the leader begins the shape perturbation, a timer starts. When this timer reaches t_{com} , the leader stops moving and sends a message to its first follower to turn it into the new leader. This triggers a repeat of the perturbation procedure, which then propagates through the chain.

The result of this propagating shape perturbation is a shift in the center of gravity of the aggregate that triggers a rolling or crawling motion sustained by the aggregate's inertia.

Acknowledgments

This work was funded by NSF grant EFMA-1830939, "EFRI C3 SoRo: Design Principles for Soft Robots Based on Boundary Constrained Granular Swarms". We thank Marc Berthoud for help with software development.

References

1. Y. Gao, S. Chien. Review on space robotics: Toward top-level science through space exploration. *Sci. Robot.* 2, eaan5074 (2017).
2. M. A. McEvoy, N. Correll. Materials that couple sensing, actuation, computation, and communication. *Science* 347, 6228, 1261689 (2015).
3. J .Romanishin, K .Gilpin, D .Rus. M-Blocks: Momentum-driven, Magnetic Modular Robots. *IEEE/RSJ International Conference on Intelligent Robots and Systems*, Tokyo, Japan, 4288-4295 (2013).

4. J .Romanishin, K .Gilpin, S. Claici, D .Rus. 3D M-Blocks: Self-reconfiguring Robots Capable of Locomotion via Pivoting in Three Dimensions. *IEEE International Conference on Robotics and Automation (ICRA)*, Seattle, WA, USA, 1925-1932 (2015).
5. B. Piranda, J. Bourgeois Designing a quasi-spherical module for a huge modular robot to create programmable matter. *Autonomous Robots* 42, 1619-1633 (2018).
6. G. Liang, H. Luo, M. Li, H. Qian, T. L. Lam. FreeBOT: A Freeform Modular Self-reconfigurable Robot with Arbitrary Connection Point - Design and Implementation *IEEE/RSJ International Conference on Intelligent Robots and Systems (IROS)*, Las Vegas, NV, USA, 2020, 6506-6513 (2020).
7. E. Brown, N. Rodenberg, J. Amend, A. Mozeika, E. Steltz, M. R. Zakin, H. Lipson, and H. M. Jaeger. Universal Robotic Gripper based on the Jamming of Granular Material. *Proc. Natl. Acad. Sci. U.S.A* 107, 44, 18809-18814 (2010).
8. P. Polygerinos, Z. Wang, K. C. Galloway, R. J. Wood, C. J. Walsh. Soft robotic glove for combined assistance and at-home rehabilitation. *Rob. Auton. Syst.* 73, 135-143 (2015).
9. T. Proietti, C. O'Neill, C. J. Hohimer, K. Nuckols, M. E. Clarke, Y. Meng Zhou, D. J. Lin, C. J. Walsh. Sensing and Control of a Multi-Joint Soft Wearable Robot for Upper-Limb Assistance and Rehabilitation. *IEEE Robotics and Automation Letters* 6, 2, 2381-2388 (2021).
10. M. Gazzola, L. H. Dudte, A. G. McCormick, L. Mahadevan. Forward and inverse problems in the mechanics of soft filaments. *R. Soc. open sci.* 5, 171628 (2018).
11. S. Li, D. M. Vogt, D. Rus, R. J. Wood. Fluid-driven origami-inspired artificial muscles. *Proc. Natl. Acad. Sci. U.S.A* 114, 50, 13132-13137 (2017).

12. J. Paik, B. An, D. Rus, and R. J. Wood. Robotic origamis: self-morphing modular robots. *Proc. 2nd Int. Conf. on Morphological Computation*, Venice, Italy, Sept., (2011).
13. M. T. Tolley, R. F. Shepherd, B. Mosadegh, K. C. Galloway, M. Wehner, M. Karpelson, R. J. Wood, G. M. Whitesides. A Resilient, Untethered Soft Robot. *Soft Robot.* 1, 3, 213-223 (2014).
14. L. L. Howell, S. P. Magleby, B. O. Olsen. Handbook of Compliant Mechanisms. *John Wiley & Sons*, New York, NY, (2013).
15. S. Felton, M. Tolley, E. Demaine, D. Rusand, R. Wood. A method for building self-folding machines. *Science* 345, 6197, 644-646 (2014).
16. E. T. Roche, M. A. Horvath, I. Wamala, A. Alazmani, S. E. Song, W. Whyte, Z. Machaidze, C. J. Payne, J. C. Weaver, C. J. Walsh Soft robotic sleeve supports heart function. *Sci. Transl. Med.* 9, 373, eaaf3925 (2017).
17. T. Vicsek, A. Zafeiris. Collective motion. *Phys. Rep.* 517, 3-4, 71-140 (2012).
18. A. Attanasi, A. Cavagna, L. Del Castello, I. Giardina, T.S. Grigera, A. Jelic, S. Melillo, L. Parisi, O. Pohl, E. Shen, M. Viale. Information transfer and behavioural inertia in starling flocks. *Nat. Phys.* 10, 9, 691-696 (2014).
19. M. Dorigo, G. Theraulaz, V. Trianni. Reflections on the future of swarm robotics. *Sci. Robot.* 5, eabe4385 (2020).
20. G. Caprari, T. Estier, R. Siegwart. Fascination of down scaling - Alice the sugar cube robot. *Journal of Micromechatronics* 1, 177-189 (2001).
21. L. Giomi, N. Hawley-Weld, L. Mahadevan. Swarming, swirling and stasis in sequestered bristle-bots. *Proc R Soc A* 469, 20120637 (2013).

22. M. Y. Ben Zion, N. Bredeche, O. Dauchot. Morphological computation and decentralized learning in a swarm of sterically interacting robots. *Sci. Robot.*, 8, 75, eabo614 (2023).
23. M. Rubenstein, A. Cornejo, R. Nagpal. Programmable self-assembly in a thousand-robot swarm. *Science* 345, 6198, 795-799 (2014).
24. J. Werfel, K. Petersen, R. Nagpal. Designing Collective Behavior in a Termite-Inspired Robot Construction Team. *Science* 343, 6172, 754-758, (2014).
25. H. M. Jaeger. Toward Jamming by Design. *Soft Matter* 11, 12-27 (2015).
26. E. Steltz, A. Mozeika, J. Rembisz, N. Corson, H. M. Jaeger. Jamming as an Enabling Technology for Soft Robotics. *Proc. SPIE 7642, Electroactive Polymer Actuators and Devices*, 764225, (2010).
27. N. Cheng, M. B. Lobovsky, S. J. Keating, A. M. Setapen, K. I. Gero, A. E. Hosoi, K. D. Iagnemma. Design and Analysis of a Robust, Low-cost, Highly Articulated Manipulator Enabled by Jamming of Granular Media. *IEEE International Conference on Robotics and Automation (ICRA)*, St. Paul, Minnesota, USA, 4328-4333 (2012).
28. M. Cianchetti, T. Ranzani, i. Gerbon, T. Nanayakkara, K. Althoefer, P. Dasgupta, and A. Menciassi. Soft Robotics Technologies to Address Shortcomings in Today's Minimally Invasive Surgery: The STIFF-FLOP Approach. *Soft Robot.*, 1, 122-131 (2014).
29. H. T. Tramsen, A. E. Filippov, S. N. Gorb, L. Heepe. Maximizing Friction by Passive Jamming. *Adv. Mater. Interfaces* 7, 1901930 (2020).
30. B. Akta, Y. S. Narang, N. Vasios, K. Bertoldi, R. D. Howe. A Modeling Framework for Jamming Structures. *Adv. Funct. Mater.* 31, 2007554 (2021).

31. Y. Wang, L. Li, D. Hofmann, J. E. Andrade, C. Daraio. Structured fabrics with tunable mechanical properties. *Nature* 596, 238-243 (2021).
32. A. S. Meeussen, J. Paulose, V. Vitelli. Geared Topological Metamaterials with Tunable Mechanical Stability. *Phys. Rev. X* 6, 041029 (2016).
33. L. A. Shaw, S. Chizari, M. Dotson, Y. Song, J. B. Hopkins. Compliant rolling-contact architected materials for shape reconfigurability. *Nat. Com.* 9, 4594 (2018).
34. X. Fang, J. Wen, L. Cheng, D. Yu, H. Zhang, P. Gumbsch. Programmable gear-based mechanical metamaterials. *Nat. Mat.* 21, 8, 869-876 (2022).
35. W. Savoie, T. A. Berrueta, . Jackson, A. Pervan, R. Warkentin, S. Li, T. D. Murphey, K. Wiesenfeld, D. I. Goldman. A robot made of robots: Emergent transport and control of a smarticle ensemble. *Sci. Robot.*, 4, 34, eaax4316 (2019).
36. S. Li, R. Batra, D. Brown, H. D. Chang, N. Ranganathan, C. Hoberman, D. Rus, H. Lipson. Particle robotics based on statistical mechanics of loosely coupled components. *Nature* 567, 361-365 (2019).
37. M. Agrawala, S. C. Glotzer. Scale-free, programmable design of morphable chain loops of kilobots and colloidal motors. *Proc. Natl. Acad. Sci. U.S.A* 117, 16, 8700-8710 (2020).
38. S. Li, B. Dutta, S. Cannon, J. J. Daymude, R. Avinery, E. Aydin1, A. W. Richa, D. I. Goldman, D. Randall. Programming active cohesive granular matter with mechanically induced phase changes. *Sci. Adv.* 7, 17, eabe8494 (2021).
39. M. A. Karimi, V. Alizadehyazdi, H. M. Jaeger, M. Spenko. A Self-Reconfigurable Variable-Stiffness Soft Robot Based on Boundary-Constrained Modular Units. *IEEE Transactions on Robotics* 38, 810-821 (2022).

40. A. J. Ijspeert, A. Crespi, D. Ryczko, J. M. Cabelguen. From Swimming to Walking with a Salamander Robot Driven by a Spinal Cord Model. *Science* 315, 5817, 1416-1420 (2007).
41. W. Zhou, Z. Hao, N. Gravish. Collective Synchronization of Undulatory Movement through Contact. *Phys. Rev. X* 11, 031051 (2021).
42. M. Brandenbourger, C. Scheibner, J. Veenstra, V. Vitelli, C. Coulais. Limit cycles turn active matter into robots. *Arxiv*, <https://arxiv.org/pdf/2108.08837.pdf>
43. W. Wen, X. Huang, S. Yang, K. Lu, P. Sheng. The giant electrorheological effect in suspensions of nanoparticles. *Nat. Mater.*, 2, 727-730, (2003).
44. Taking as a typical load $\Gamma_{1,i} = mgr$, the torque applied to a unit's active rotor of radius r by the weight of a neighboring unit at right angle with respect to gravity, we use Eq. 4 to find $\eta_{\text{eff}} = (1 + \alpha)\eta_0 \frac{mgr}{mgr - k(u^* - |u|)}$.
45. P. Oswald Rheophysics: The Deformation and Flow of Matter *Cambridge University Press* (2009).
46. When the u_i across all units have the same sign regardless of Γ_f , hysteresis is still observed in the regime colored red in Fig. 3, but it will be either negative (plasticity) or positive depending on the sign of the load. As a consequence, the transition toward the self-oscillating regime (orange in Fig. 3) can be shifted slightly. We still observe self-organized oscillating states, but units oscillate sinusoidally regardless of α , with a shift of the equilibrium angle $\Delta\theta_0 = k(u - u^*)/G$. This is due to alternating within an oscillations between a friction in the direction of the bias, and a friction in the opposite one.
47. J. Bongard, V. Zykov, H. Lipson. Resilient Machines Through Continuous Self-Modeling. *Science* 314, 5802, 1118-1121 (2006).

48. N Cheney, R MacCurdy, J Clune, H Lipson. Unshackling evolution: evolving soft robots with multiple materials and a powerful generative encoding. *ACM SIGEVOlution* 7, 1, 11-23 (2014).
49. A. Hughes, B. Drury. Electric Motors and Drives, Fundamentals, Types and Application. *Newnes - Elsevier* (1990), 4th Ed., (2013).
50. H. C. H. Chiu, M. Rubenstein, W. M. Shen. “Deformable wheel” - a self-recovering modular rolling track. *Distributed Autonomous Robotic Systems 8*, edited by H. Asama, H. Kurokawa, J. Ota, and K. Sekiyama (Springer Berlin Heidelberg, Berlin, Heidelberg), 429-440 (2009).
51. O. Peleg, J. M. Peters, M. K. Salcedo, L. Mahadevan. Collective mechanical adaptation in honeybee swarms. *Nat. Phys.* 14, 1193-1198 (2018).